J Mater Sci: Mater Electron (2022) 33:19937–19946

Study on the DC supply and charging effect on the growth of carbon nanotubes and their electrochemical properties

S. Chetana[1,2], Manjunath Shetty[4], Kunal Roy[1], Jagadeesh Babu Sriramoju[3], Guddappa Halligudra[1], Prasanna D. Shivaramu[1], C. S. Ananda Kumar[1], K. G. Basavakumar[5,*], and Dinesh Rangappa[1,*]

[1] *Department of Applied Sciences (Nanotechnology), Center for Postgraduate Studies, Visvesvaraya Technological University, Muddenahalli, Chikkaballapur, Karnataka 562101, India*

[2] *Research and Development Department, Uttaranchal University, Arcadia Grant, Chandanwari, Prem Nagar, Dehradun, Uttarakhand 248007, India*

[3] *Department of Physics, Malla Reddy Engineering College (A), Secunderabad, Telangana 500100, India*

[4] *Department of Aeronautical and Automobile Engineering, Manipal Institute of Technology, Manipal Academy of Higher Education (MAHE), Manipal 576104, Karnataka, India*

[5] *C Byregowda Institute of Technology, Kolar 563101, Karnataka, India*

Received: 23 March 2022
Accepted: 21 July 2022
Published online: 26 August 2022

ABSTRACT

Preparation of chirality-defined few-walled CNT (FWCNT) is one of the major challenges in the carbon nanotube (CNT) fields. In the last two decades, significant progress has been made in preparing chirality-controlled synthesis (CCS) of FWCNT through both a direct synthesis approach and a post-synthesis separation approach due to insignificant changes in the tube diameter and twist angle. Hopefully, the present study will encourage further research on the preparation of FWCNT and also utilize key research and practical applications of FWCNTs. In this study, the SEM images of as-grown nanotubes show that applying electric field during the growth process affects the growth of the nanotubes and nanotubes properties can be achieved and altered by changing the supplied electrical DC bias. Raman spectroscopy has been used to analyze the structure and forms of grown FWCNTs samples. The Raman spectrum from all obtained CNTs samples shows the presence of major two peaks, corresponding to the 1350 cm^{-1} and 1570 cm^{-1} bands as well as characteristic Raman bands for metallic or semi-conductive CNTs and their corresponding electrochemical performance also have been performed.

Address correspondence to E-mail: bkumarkg@gmail.com; dinesh.rangappa@vtu.ac.in

https://doi.org/10.1007/s10854-022-08813-6

1 Introduction

Carbon nanotube (CNT)-based devices have been produced consecutively, which implies a bright future for CNT electronics and arouses the desire for direct growth of identical semiconducting CNTs together with the semiconductor industry standard. For various approaches to control the chirality of CNTs, the solution is to deepen the understanding of the growth mechanism in chemical vapor deposition. A physical picture focused on carbon atoms transfer in CVD growth of CNTs has been established for two decades. However, the charge transfer in the growth process can be systematically studied [1].

In the last 15 years, chirality control is considered the biggest challenge in this area of research which is related to the initiation of graphitization of CNTs [2]. When the catalytic substrate bonding reaction is weak, hydrocarbon decomposition occurs at the top of the metal surface having a sharp contact angle with the substrate. The hydrocarbon (C_2H_2) spreads down through the metal and the CNTs precipitate from the bottom, pushing the metal particles from the substrate to the tip of the CNTs, which then precipitate from the bottom, while the upper part of the CNTs continues the C_2H_2 decomposition. This model is known as Tip Growth Model [3]. Subsequent hydrocarbon deposition takes place in the lower peripheral surface of the metal and dissolved carbon diffuses upward, while the CNTs grow with the catalyst particle in their base. Such a mechanism is named the base-growing model [3].

Recent advances in the selective synthesis of SWCNT by epitaxial growth model [4], in this same mechanism same other SWCNTs synthesis by bimetallic catalyst (7–8), and also same other techniques used to control mechanisms magnetic field [5] and electric field to control the chirality of SWCNTs. This model faced main challenges of catalyst size, chirality specific growth [4], and stability of the nanosize SWCNTs growth processes. The key to the various approaches to controlling the chiral index of CNTs is to expand our understanding of the mechanisms of catalytic growth in chemical vapor deposition. We recently reported on CNT's vertical growth by serving magnetic and electric fields [5] but hear difficulty for chirality controlling also we reported the development of SWCNTs by novel electric field controlling mechanism and also by changing the orientation of the substrate concerning the direction of the electric field or by applying an electric current during the growth process, the desired carbon nanotubes are formed.

The generation of charge during the growth formation of CNTs has already been studied and reported preciously. But the variation in applied DC bias and its effects on the resistive behavior during the growth of CNTs and their electrochemical properties have not been studied previously. Herein, we investigated the effect of DC voltage on Fe/Al-catalyzed CNT growth, their properties (including semiconductive, or metallic), and their electrochemical properties also. The additional electrons arise from the generation and transfer of charge during the growth of CNTs, indicating that electrochemical processes take place during the surface reaction step. The field measurement equipment was then subsequently designed to confirm that CNT's CVD growth could be considered a basic battery system. Moreover, it was found that changes in Fermi levels in Fe–Al-based catalysts have a significant effect on the chirality of CNTs when different external electric fields were applied. These discoveries not only provide new insights into the growth of CNTs but also open up new possibilities to control the growth of CNTs using electrochemical methods.

2 Methodology

2.1 Catalyst preparation

Catalyst preparation was carried out by the simple sol–gel method, as reported elsewhere [6]. 0.5 (M) of $Fe(NO_3)_3{\cdot}9H_2O$ was added into 100 ml deionized water and stirred for 30 min to get a clear homogeneous solution followed by the addition of 0.8 (M) of $Al(NO_3)_3{\cdot}9H_2O$. The whole solution mixture was initially stirred at room temperature for 24 h and 12 h more at 90 °C to get dried material. Finally, the dried sample was annealed at 450 °C to obtain a Fe_2O_3/Al_2O_3 catalyst.

2.2 CNTs growth mechanism

The furnace (KejiaFurnace KJ-1600G) temperature was increased to 950 °C to grow CNTs, with a ramp rate of 10 °C/min with an Ar atmosphere containing 5% H_2 with a flow rate of 100 sccm, followed by 100 sccm of C_2H_2 gas was supplied to initiate the growth.

Finally, after growing for 60 min, the sample was cooled down to room temperature gradually. During the CVD process, the growth of CNT may follow the following mechanism as reported elsewhere [4, 6, 7].

2.2.1 Phase 1

Initially, near 500–600 °C, the Fe_2O_3 phase gets changed into unstable α-Fe_2O_3 and then gets reduced to α-Fe_3O_4 by absorbing some moisture content. After phase change, the unstable α-Fe_3O_4 again transformed into α-Fe_2O_3 by reaching the growth temperature at 700 °C with increasing crystallinity.

$$Fe_2O_3 \xrightarrow{500-600^{\circ}C} \alpha - Fe_2O_3 \xrightarrow{H_2O} \alpha - Fe_3O_4 \sim \xrightarrow{700^{\circ}C} \alpha - Fe_2O_3 \quad (1)$$

2.2.2 Phase 2

Above 800 °C, both α-Fe_2O_3 and acetylene start to decompose because of the reduction of α-Fe_2O_3 into its unstable Fe_3O_4 phase by hydrogen atoms (from C_2H_2) (Eq. 2). The reduced unstable Fe_3O_4 instantly transformed into metallic α-Fe according to Eq. (3). Similarly, Al_2O_3 has also been converted into metallic α-Al because of the temperature increment above 900 °C, since Al_2O_3 gets reduced at higher temperature of 900–950 °C as shown in Eq. (4).

$$C_2H_2 \xrightarrow{800^{\circ}C} 2C + 2H \quad (2)$$

$$3\alpha - Fe_2O_3 \xrightarrow{2H,900^{\circ}C} 2\alpha - Fe_3O_4 + H_2O \rightarrow \alpha - Fe \quad (3)$$

$$Al_2O_3 \xrightarrow{950^{\circ}C} \alpha - Al_2O_3 \xrightarrow{H,950^{\circ}C} \alpha - Al \quad (4)$$

2.2.3 Phase 3

In the final phase, decomposed C atoms meltdown and nucleation were initiated after reaching supersaturation level on the surface of α-Fe and α-Al to form Fe–C and Al–C orientation followed by the transformation into their carbides (such as Fe_3C and Al_4C_3), respectively. Consequently, CNTs growth was also confirmed via precipitation according to Eqs. (5–6).

$$\alpha - Fe + C \xrightarrow{800-900^{\circ}C} Fe - C \xrightarrow{2Fe,800-900^{\circ}C} Fe_3C \quad (5)$$

$$\alpha - Al + C \xrightarrow{>900^{\circ}C} Al - C \xrightarrow{3Al/2C,>900^{\circ}C} Al_4C_3 \quad (6)$$

Thus, by the combined catalytic effect of Fe_2O_3/Al_2O_3 catalysts, the controlled growth and formation of CNTs can be carried out because Fe_2O_3 helps to catalyze the reaction up to 800 °C and Al_2O_3 helps to catalyze the reaction above 900 °C in a suitable way.

a. In situ power supply installation and measurement

During the growth reaction, in situ measurement of DC electrical bias influence on CNT (double-walled and multi-walled) synthesis has been carried out using a continuous DC power supply (VRR 3002). The growth of double-walled and multi-walled CNTs was examined within the bias range from 0.5 to 3.5 V having 0.5 V of increment. By minimizing environmental noise and connecting Keithley 2401 sourcemeter, charge generation on the surface of CNTs has been observed in terms of electrical resistance at different biases which was quite similar to the traditional emf measurement (Fig. 1).

3 Results and discussion

Figure 2 represents the variation of resistance on CNTs growth and temperature effect on the process. It was observed that initially, the resistance decreased with increasing temperature from room temperature to 950 °C (operating temperature) which was according to the Ohmic rule. Since the substrate surface and oxide catalysts were both semi-conductive, resistance came down with a steeper profile up to an initial 190 min. After reaching the operating temperature (950 °C), 100 sccm Ar/H_2 flow was begun and it was found that the resistance became stable for 20 min. But as the 100 sccm C_2H_2 was added as a feed gas into the reaction chamber at 60 min, the resistance again started to come down slowly and after an hour, a 0.0002 Ω of resistance was dropped. This gradual resistance drop phenomenally attributes to the growth of semi-conductive CNTs.

The diffraction pattern of few-walled CNT is displayed in Fig. 3. The major characteristic peaks of the few-walled CNT samples were observed at 2θ (deg.) of 26.25, 53.8, and 57.2° corresponding to the lattice planes (h k l) of (0 0 2), (0 0 4), and (1 0 2), respectively, with a hexagonal arrangement [8]. Peak position at 31.87° corresponding to the Al_4C_3 at (2 0 1) plane [9]. The diffraction peak at 43.1° indicated the presence of α-Fe_2O_3 corresponding to the (0 1 1) plane [10]. The peak at 36° corresponds to the (1 1 1) plane was of γ″-FeN [11]. Diffraction peak at 37.6° was

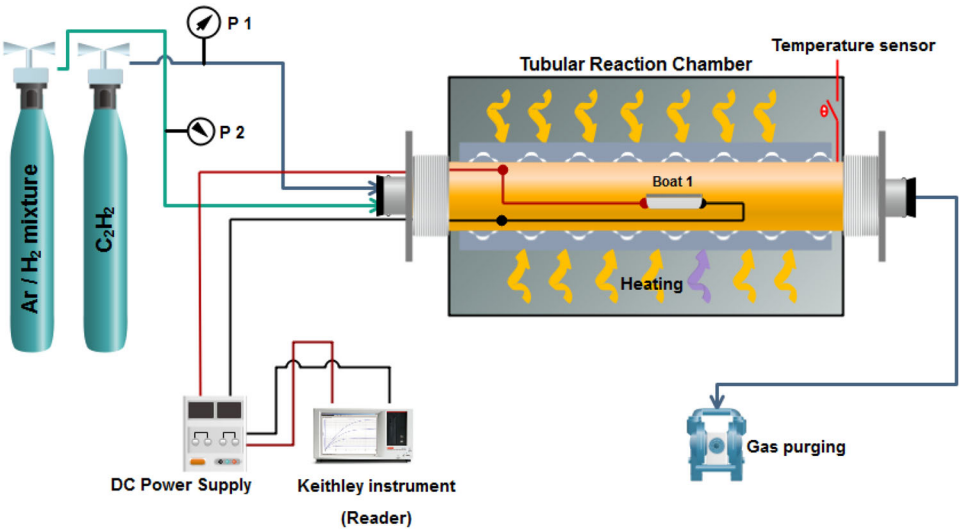

Fig. 1 Schematic of in situ DC supply-assisted chemical vapor deposition technique for the synthesis of CNTs

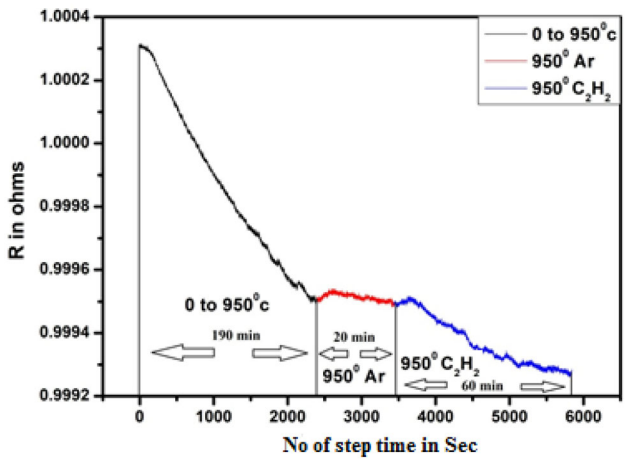

Fig. 2 In situ measurement of DC bias on CNTs growth showing the change of electrical resistance with feed gas

attributed to Fe_3C at (2 2 1) [9]. 44.75° was attributable to the α-Fe and Fe_3C overlapping at (1 1 0) and (2 2 0) planes and 63° was attributed to the appearance of α-Fe at the (2 0 0) [9]. A peak at 66° was corresponding to α-Al_2O_3 at the (4 4 0) plane [12]. In Fig. 4, it has been observed that the major characteristic diffraction peak of as-synthesized CNTs has been shifted slightly by lowering the applied potential which signifies the enhancement of growth of semi-conductive few-walled CNTs at lesser resistance [13].

The FTIR spectral illustration is displayed in Fig. 5. It showed the presence of weak vibration of α-Fe_2O_3 and α-Al_2O_3 phases between 500 and 700 cm^{-1} [14] and also it revealed that the samples are not

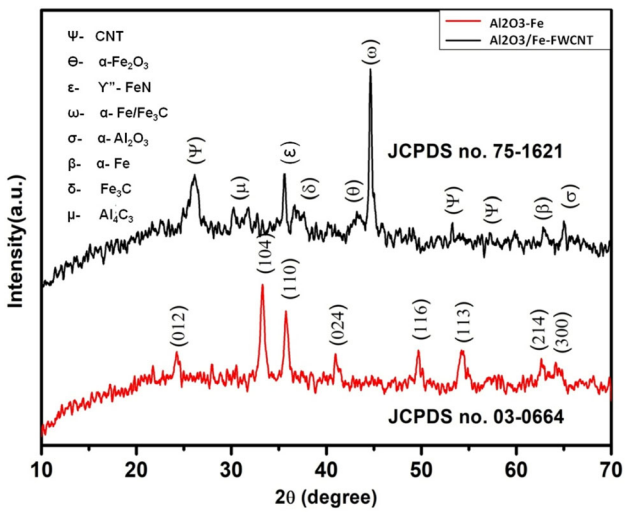

Fig. 3 XRD pattern of CNT, including metal carbides and nitride

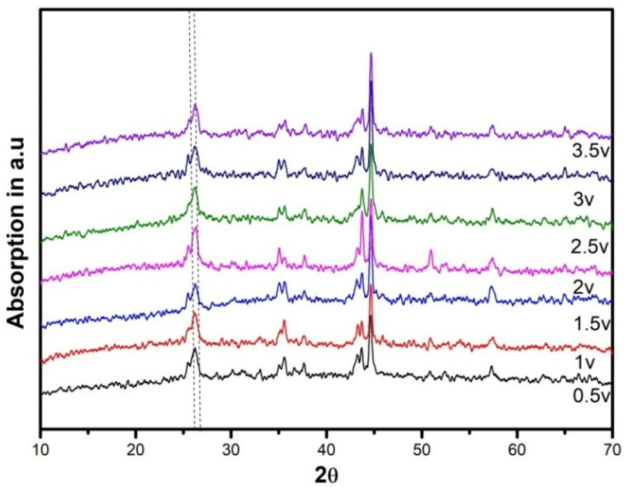

Fig. 4 Diffraction patterns of CNTs synthesized at different applied electrical biases

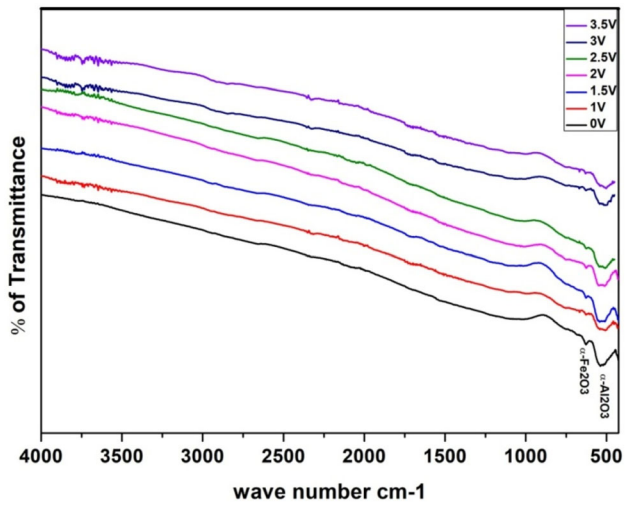

Fig. 5 FTIR spectral profiles of CNTs synthesized at different applied electrical biases

functionalized, i.e., pure CNTs. Some peaks appearance has been observed near 3700 cm^{-1} attributable to the presence of surface hydroxyl groups (–OH) because of the absorption of atmospheric moisture [15].

Figure 6 displays the recorded Raman profiles of FWCNT samples synthesized at different applied electrical biases from 0 to 3.5 V indicating the presence of characteristic peak intensities of RBM (radial breathing mode) (Fig. 6b and d) and G-band. However, RBM is a distinct quantum characteristic of SWCNT because of their radial vibration, and it cannot be overlooked for FWCNTs completely because of their diameters below 2 nm [16]. Moreover, the RBM is strongly correlated with the tube diameter distribution which can be extracted using the following relation [17]:

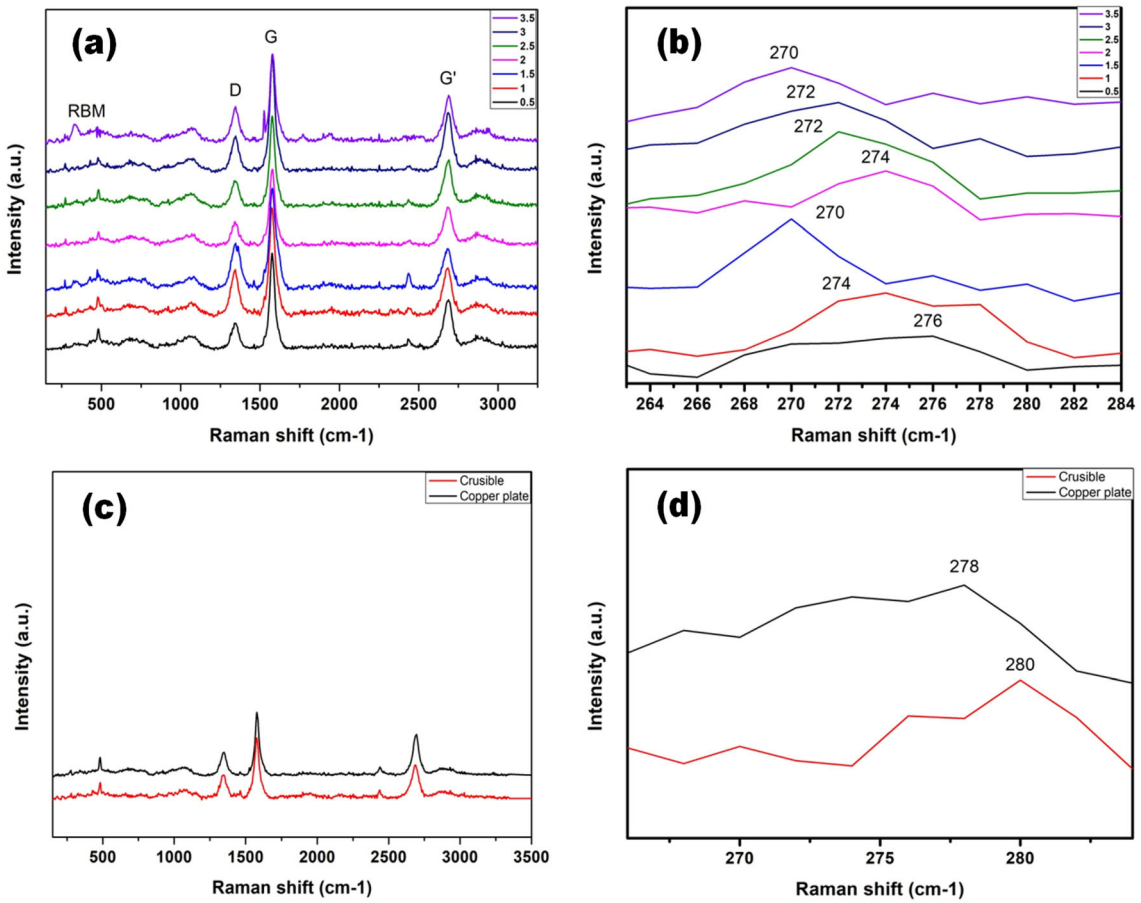

Fig. 6 Raman spectra of FWCNTs **a** synthesized at different applied potentials, **b** RBM regions at different applied potentials, **c** synthesized in alumina crucible and copper plate, respectively, and **d** RBM regions for alumina and copper plate-synthesized FWCNTs

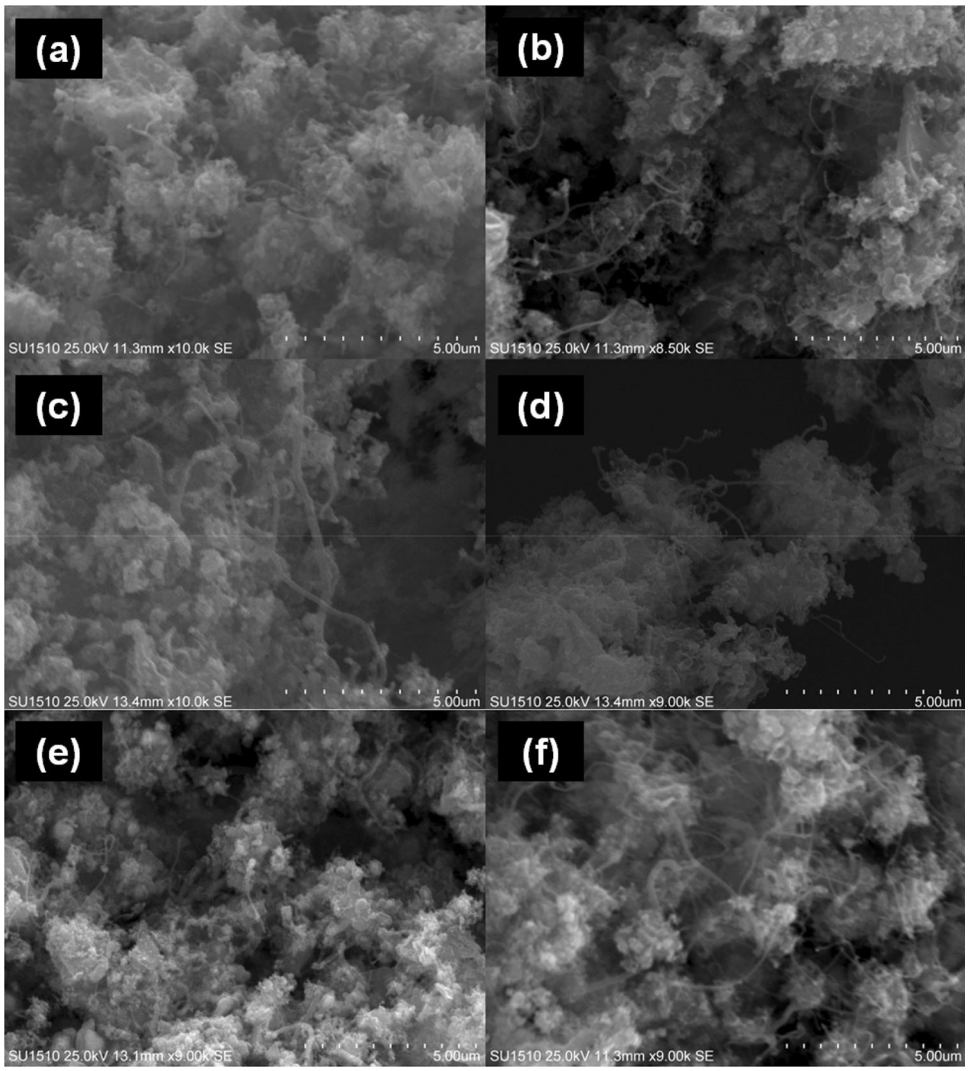

Fig. 7 SEM photographs of entangled CNTs bundles synthesized at **a** 0.5 V, **b** 1.0 V, **c** 1.5 V, **d** 2.0 V, **e** 2.5 V, and **f** 3.0 V

$$f_{\mathrm{RBM}} = \frac{c_1}{d_{\mathrm{CNT}}} + c_2 \tag{7}$$

where f is the frequency of RBM (cm^{-1}), d_{CNT} is the diameter of CNT (nm), and c_1 and c_2 are constants having the value of 235 (cm^{-1} nm) and 9 (cm^{-1}), respectively. From Fig. 6a and c, it can be observed that the D-band and G-band resonated near 1350 cm^{-1} and 1570 cm^{-1} in all the spectrums with the D/G ratio ranging between 0.4 and 0.5 representing the graphitization of the samples with the good agreement [18]. With increasing applied potential, the average diameter of the FWCNTs also increased gradually from 0.87 to 0.9 nm because of the redshift of the RBM region which was estimated using Eq. (7). Most importantly, a strong characteristic peak of the BWF band (Breit–Wigner–Fano) was found at a higher electrical bias (3.5 V) near 1535 cm^{-1} frequency which was attributed to the formation of metallic CNT [19]. Further, the inclusion of G′-bathe nd nandr 2700 cm^{-1} intensified the formation of fewer walls as well as the metallicity of the FWCNTs [16].

Figure 7a–f displays the SEM photographs of as-synthesized CNTs at different applied potentials; hence, densely entangled nanotubes were observed in all the images which were likely to be strongly connected bundles of ropes as shown. Aggregation and compaction of these nanotubes may be enhanced by the strong Van der Waal's interaction and π–π stacking [20, 21].

The electron transfer efficiency, i.e., redox efficiency by exchanging cation–anion between electrolyte and electrode material is mainly analyzed by cyclic voltammetry. In the particular potential window, these redox phenomena get influenced by the

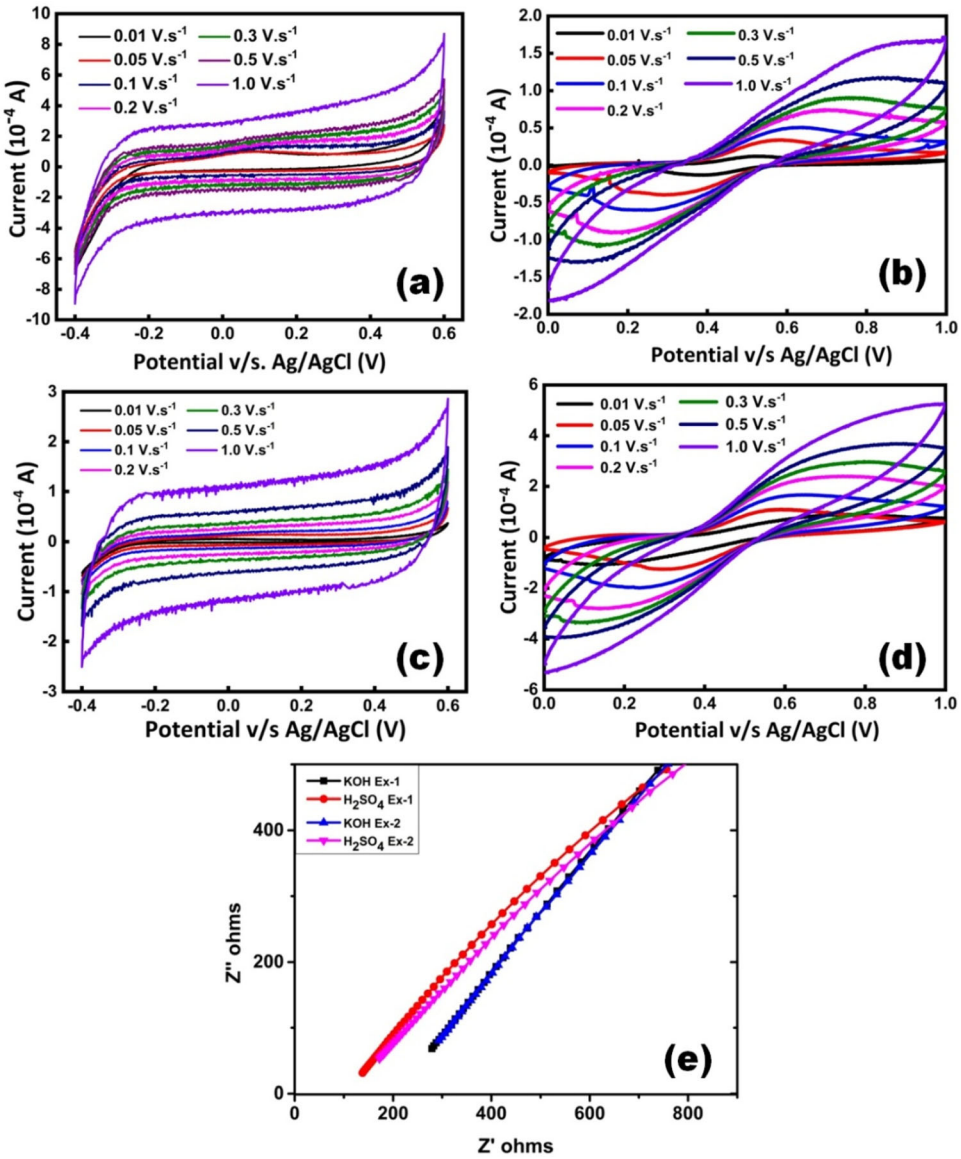

Fig. 8 Cyclic voltammograms of electrode material using **a** CNT synthesized at 0 V and 1(M) KOH electrolyte, **b** CNT synthesized at 0 V and 1(M) H_2SO_4 electrolyte, **c** CNT synthesized at 3.5 V and 1(M) KOH electrolyte, **d** CNT synthesized at 3.5 V and 1(M) H_2SO_4 electrolyte, and **e** electrochemical impedance (Nyquist) plot for CNT-based capacitive electrode at different electrolytes

Table 1 The specific capacitance of CNT-based electrodes at different electrolyte and scan rates

Scan rate (V s^{-1})	Specific capacitance (F g^{-1})			
	CNT-0 V		CNT-3.5 V	
	H_2SO_4	KOH	H_2SO_4	KOH
0.01	67.167	49.473	70.436	18.288
0.05	1.134	1.39	38.144	0.094
0.1	2.099	0.771	5.092	0.142
0.2	1.622	0.627	5.507	0.121
0.3	1.503	0.587	4.798	0.141
0.5	1.018	0.449	3.184	0.12
1	0.579	0.272	1.721	0.098

electron cloud density and based on that energy storage capability of a material can be explored. CV measurements of CNTs synthesized at 0 V and 3.5 V against Ag/AgCl standard electrode and two different electrolyte solutions are (KOH and H_2SO_4) as shown in Fig. 8a–d within the potential window of − 0.4 to 6.0 V (for KOH electrolyte) and 0 V to 1.0 V (for H_2SO_4 electrolyte) at the different scan rates from 0.01 to 1.0 V s^{-1}. In both the cases of CNT-0 V and 3.5 V, it can be observed that CV profiles for KOH electrolytes (Fig. 8a and c) are quite smooth compared to H_2SO_4-based electrolytes (Fig. 8b and c). This implies a very less oxidation–reduction reaction happening between electrolyte and CNTs which can be reflected from the specific capacitance value

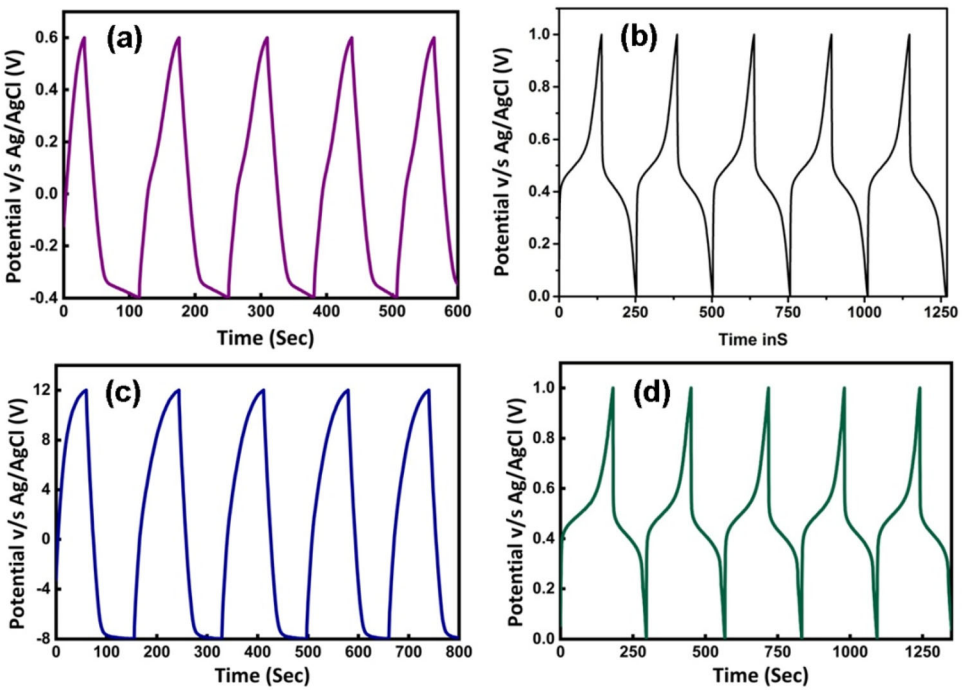

Fig. 9 Charge–discharge profiles of **a** CNT synthesized at 0 V and 1(M) KOH electrolyte, **b** CNT synthesized at 0 V and 1(M) H_2SO_4 electrolyte, **c** CNT synthesized at 3.5 V and 1(M) KOH electrolyte, and **d** CNT synthesized at 3.5 V and 1(M) H_2SO_4 electrolyte

(KOH) in Table 1 also. The reason might be the generation of lesser numbers of electrons and less interaction on the surface of CNTs compare to H_2SO_4. Furthermore, in both the CV profiles of H_2SO_4-based electrolytes, small oxidation–reduction peaks were observed at 0 to 0.2 V and 0.8 to 1.0 V. Impedance profiles of the CNT-electrodes in Fig. 8e confirmed the pseudocapacitive nature of the material which supported the literature report also [22] having strong possibilities of development of the CNTs and CNT-based materials for the application of electrochemical energy storage system. Charge–discharge performances in Fig. 9a–d also supported the previous literature with the good agreement of possible development of pseudocapacitor [22].

4 Conclusion

In this study, we have observed the changes in the CNT growth phase and its physicochemical properties with the variation of applied DC potential from 0.5 to 3.0 V. At higher potential (> 3.0 V), it was found that the metallic CNT was formed and below 3.0 V, semi-conductive CNTs were grown. All the Raman spectral analyses have supported the formation of a FWCNT because of the presence of a very weak RBM region attributing the predictive diameter approx. below 1.5 nm. The electrochemical performance showed the possibility of application of synthesized FWCNTs in semiconductor-based energy storage systems. Thus, the improvement and growth-controlled CNTs synthesis with desired chirality can be deemed in upcoming time with specific findings and new species. The main focus of this study was to investigate the effect of applied DC bias during the growth of CNTs in its semi-conductive and metallic formation and their corresponding effect on the electrochemical energy storage system (supercapacitor), which has been successfully represented. These discoveries not only provide new insights into the growth of CNTs but also open up new possibilities to control the growth of CNTs depending on the requirement for the application in electrochemical energy storage systems.

Acknowledgements

The authors would like to acknowledge the Department of IT, BT and S&T, Government of Karnataka for sponsoring the research work under VGST, CESEM 18.2. The authors also like to acknowledge the Research & Development Cell, Uttaranchal University for carrying out some characterizations.

Author contributions

All authors equivalently contributed to the study, conception, and methodological designing of the present work. Materials preparation, data collection, measurement, and analysis have been carried out by CS, MS, KR, and MM. Draft of the manuscript was written by CS and KR. Modifications, new insertions, commenting, and reviews were done by MS, VG, JSB, GH, PDS, and AKCS. The work has been supervised and monitored by KGB and DR.

Funding

Funding was provided by the Department of Science and Technology for Social Development (Grant No. VGST, CESEM 18.2).

Data availability

All the data generated and analyzed during this study were included in this article during its preparation.

Declarations

Conflict of interest The authors declare no conflict of interest.

References

1. M.P. Kumar, S. Raga, S. Chetana, D. Rangappa, Realization of anomalous microwave absorption characteristics of PVB-PEDOT:PSS with electromagnetic data-driven discovery. IEEE Trans. Dielectr. Electr. Insul (2022). https://doi.org/10.1109/TDEI.2022.3148440
2. E. Plaza, H. Briceño-Fuenmayor, J. Arévalo, R. Atencio, L. Corredor, Electric field effect in the growth of carbon nanotubes. J. Nanopart. Res. (2015). https://doi.org/10.1007/s11051-015-3055-9
3. R.T.K. Baker, M.A. Barber, P.S. Harris, F.S. Feates, R.J. Waite, Nucleation and growth of carbon deposits from the nickel catalyzed decomposition of acetylene. J. Catal. (1972). https://doi.org/10.1016/0021-9517(72)90032-2
4. F. Yang, X. Wang, D. Zhang, J. Yang, D. Luo, Z. Xu, J. Wei, J.Q. Wang, Z. Xu, F. Peng, X. Li, R. Li, Y. Li, M. Li, X. Bai, F. Ding, Y. Li, Chirality-specific growth of single-walled carbon nanotubes on solid alloy catalysts. Nature (2014). https://doi.org/10.1038/nature13434
5. M. Baghgar, Y. Abdi, E. Arzi, Effects of magnetic and electric fields on the growth of carbon nanotubes using plasma enhanced chemical vapor deposition technique. EPJ Appl. Phys. (2009). https://doi.org/10.1051/epjap/2009162
6. D.U. Zuru, Z. Zainal, M.Z. Hussein, A.M. Jaafar, H.N. Lim, S.K. Chang, Theoretical and experimental models for the synthesis of single-walled carbon nanotubes and their electrochemical properties. J. Appl. Electrochem. **48**, 287–304 (2018). https://doi.org/10.1007/S10800-018-1158-6/FIGURES/11
7. B. Liu, W. Ren, L. Gao, S. Li, S. Pei, C. Liu, C. Jiang, H.M. Cheng, Metal-catalyst-free growth of single-walled carbon nanotubes. J. Am. Chem. Soc. (2009). https://doi.org/10.1021/ja8093907
8. B.V. Mohan Kumar, R. Thomas, A. Mathew, G. Mohan Rao, D. Mangalaraj, N. Ponpandian, C. Viswanathan, Effect of catalyst concentration on the synthesis of MWCNT by single step pyrolysis. Adv. Mater. Lett. (2014). https://doi.org/10.5185/amlett.2014.592
9. V. Krisyuk, A.N. Gleizes, L. Aloui, A. Turgambaeva, B. Sarapata, N. Prudhomme, F. Senocq, D. Samélor, A. Zielinska-Lipiec, D. de Caro, C. Vahlas, Chemical vapor deposition of iron, iron carbides, and iron nitride films from amidinate precursors. J. Electrochem. Soc. (2010). https://doi.org/10.1149/1.3430105
10. W.J. Yu, P.X. Hou, L.L. Zhang, F. Li, C. Liu, H.M. Cheng, Preparation and electrochemical property of Fe_2O_3 nanoparticles-filled carbon nanotubes. Chem. Commun. (2010). https://doi.org/10.1039/c0cc02121k
11. L. Dumée, K. Sears, J. Schütz, N. Finn, M. Duke, S. Gray, Influence of the sonication temperature on the debundling kinetics of carbon nanotubes in propan-2-ol. Nanomaterials (2013). https://doi.org/10.3390/nano3010070
12. P.S. Santos, H.S. Santos, S.P. Toledo, Standard transition aluminas. Electron microscopy studies. Mater. Res. (2000). https://doi.org/10.1590/s1516-14392000000400003
13. J. Wang, P. Liu, B. Xia, H. Wei, Y. Wei, Y. Wu, K. Liu, L. Zhang, J. Wang, Q. Li, S. Fan, K. Jiang, Observation of charge generation and transfer during CVD growth of carbon nanotubes. Nano Lett. (2016). https://doi.org/10.1021/acs.nanolett.6b00841
14. P.X. Hou, C. Liu, H.M. Cheng, Purification of carbon nanotubes. Carbon N. Y. (2008). https://doi.org/10.1016/j.carbon.2008.09.009
15. M.H. Razali, A. Ahmad, M.A. Azaman, K.A.M. Amin, Physicochemical properties of carbon nanotubes (CNT's) synthesized at low temperature using Simple hydrothermal method. Int. J. Appl. Chem. **12**, 273–280 (2016)
16. M.S. Dresselhaus, G. Dresselhaus, R. Saito, A. Jorio, Raman spectroscopy of carbon nanotubes. Phys. Rep. (2005). https://doi.org/10.1016/j.physrep.2004.10.006

17. D.Y. Kim, C.M. Yang, Y.S. Park, K.K. Kim, S.Y. Jeong, J.H. Han, Y.H. Lee, Characterization of thin multi-walled carbon nanotubes synthesized by catalytic chemical vapor deposition. Chem. Phys. Lett. (2005). https://doi.org/10.1016/j.cplett.2005.07.064
18. R. Kamalakannan, K. Ganesan, S. Ilango, N. Thirumurugan, V.N. Singh, M. Kamruddin, B.R. Mehta, A.K. Tyagi, The role of structural defects on the transport properties of a few-walled carbon nanotube networks. Appl. Phys. Lett. (2011). https://doi.org/10.1063/1.3583583
19. S.M. Bose, S. Gayen, S.N. Behera, Theory of the tangential G-band feature in the Raman spectra of metallic carbon nanotubes. Phys. Rev. B (2005). https://doi.org/10.1103/PhysRevB.72.153402
20. N. Saifuddin, A.Z. Raziah, A.R. Junizah, Carbon nanotubes: a review on structure and their interaction with proteins. J. Chem. (2013). https://doi.org/10.1155/2013/676815
21. D.A. Britz, A.N. Khlobystov, Noncovalent interactions of molecules with single walled carbon nanotubes. Chem. Soc. Rev. (2006). https://doi.org/10.1039/b507451g
22. C. Zhong, Y. Deng, W. Hu, J. Qiao, L. Zhang, J. Zhang, A review of electrolyte materials and compositions for electrochemical supercapacitors. Chem. Soc. Rev. (2015). https://doi.org/10.1039/c5cs00303b